EVALUATING THE THEORY OF BONE MECHANOREGULATION IN THE PHYSIOLOGICAL LOADING SCENARIO

YONGTAO LU[*,¶], WENYING ZHAO[¶], JUNYAN LI[‡] and CHENGWEI WU[‡1,*,¶§]

[*] *State Key Laboratory of Structural Analysis for Industrial Equipment*
Dalian University of Technology, Dalian, China
[¶] *Department of Engineering Mechanics*
Dalian University of Technology, Dalian, China
[‡] *Department of Biomedical Engineering*
Middlesex University, London, UK
[§]*cwwu@dlut.edu.cn*

In this paper, the theory of bone mechanoregulation under physiological loading was evaluated. The entire right tibiae of wild type (WT, N = 5) and Parathyroid Hormone (PTH, N = 5) treated C57BL/6J female mice were scanned using an *in vivo* μCT imaging system at 14, 16, 17, 18, 19, 20, 21 and 22 weeks. The PTH intervention started from week 18 until week 22. Subject-specific finite element (FE) models were created from the μCT images and physiological loading condition was defined in the FE models. The rates of changes in bone mineral content (BMC), bone mineral density (BMD) and bone tissue density (TMD) were quantified over 40 anatomical compartments across the entire mouse tibia. The resulting values were then correlated to the average 1st principal tensile strain (ε_1) and the strain energy density (SED) for every compartment at weeks 18, 20 and 22. It was found that: in both groups, ε_1 had a minimal effect on the variability of ΔBMC ($p > 0.01$); SED had a significant effect on the variability of ΔBMC only in the WT group ($p < 0.01$); ε_1 had a significant effect on the variability of ΔBMD only in the PTH group ($p < 0.01$); SED had a significant effect on the variability of ΔBMD in both groups ($p < 0.01$); neither SED nor ε_1 had a significant effect on the variability of ΔTMD ($p > 0.01$). These results are the first to reveal the mechanism of bone mechanoregulation in the physiological loading scenario.

Keywords: Bone remodelling; mechanoregulation; principal strain; strain energy density; finite element

1. Introduction

Since the seminal work of Harold Frost in the 1960s,[1] the development of a quantitative bone mechanoregulation theory has been a central research question for many researchers in biomechanics and mechanobiology. First driven by the concerns associated with "stress shielding" in the first generation of hip prostheses,[2-5] then by the intense research on the biomechanical mechanism of bone fragility in osteoporosis,[6-8] the topic has received massive attentions in the past. In spite of all these efforts, only in the last few years, the development of *in vivo* micro computed tomography (μCT) imaging in small animals has finally enabled the non-invasive observation of bone adaptations at tissue scale *in vivo*.

There are mainly two research groups who have made extensive efforts on this topic. The first one is Ralph Mueller's research team at ETH Zurich. They combined *in vivo*

‡ Corresponding author.

mechanical loading, *in vivo* µCT imaging and image registration to monitor the remodelling of caudal vertebra [9] and for the first time it was possible to non-invasively monitor the changes in tissue morphology with an image resolution down to tissue scale (10.0 µm). Using the same experimental set-up, Schulte *et al.* showed that a model, assuming strain energy density (SED) as a mechanical stimulus, could predict well the experimental results obtained by loading the sixth caudal vertebra with a cyclic load ranging between 1.00 N and 9.00 N.[10] In a follow-up study, they further showed that the model could accurately predict the changes in BV/TV in various intervention groups including mechanical loading, Parathyroid Hormone (PTH), and bisphosphonates.[11] Recently, in another study using the same methodology, they correlated the changes in BV/TV with the mechanical stimulus of SED over six-week investigation, and found significant correlations only in the loaded mouse group, not in the control group.[12] However, it should be noted that the correlations were analysed only in the cancellous bone and the averaged properties were used, for example the bone volume fraction over the entire volume of interest (VOI).

The other group who has made extensive work on this topic is the research team at the Julius Wolff institute, Berlin. They proposed an alternative model which is similar to the one proposed by Mueller's team,[13] but they focused on mouse tibia and used a mechanical loading set-up that is similar to the one proposed by De Souza *et al*.[14] In a study where the cancellous bone in the proximal tibia and a small cortical region at the tibial midshaft were used as the VOIs, they found that mechanical loading had an anabolic effect on bone remodelling, but they could not find any correlation between the intensity of loading and the rate of bone remodelling.[15]

Most of these studies confirm the existence of some mechanoregulation mechanism for bone adaptation at the tissue scale. However, the studies which explored such mechanism all involve para-physiological loading regimes, either very high [16,17] or very low [18]. Most researchers agree that a correlation exists between the intensity of mechanical stimulus and bone adaptation under such para-physiological loading conditions. The question that remains unanswered is: does this correlation remain significant when the loading condition is close to that observed during daily life (i.e., physiological loading)? Assuming the answer is positive, the second question is: which mechanoregulation mechanism regulates bone adaptation in the physiological loading scenario?

A number of different mechanisms of bone mechanoregulation have been theorised, but the most popular theories can be clustered into two families: the first one is the theory proposing that bone cells are directly or indirectly mechanosensitive to the deformation of mineralised extracellular matrix and respond with a certain degree of proportionality to the intensity of such deformation;[19,20] and the other one is the theory proposing that any mechanical load produces more or less a microscopic damage in the mineralised extracellular matrix, which is transduced into the cellular regulation via a number of direct or indirect paracrine signallings.[21,22] From a biomechanical point of view, the deformation of the mineralised extracellular matrix and its micro-damage are closely related, and the mechanisms of paracrine signalling, in which these two theories are involved, are very different. Furthermore, people who are interested in using the theory of bone mechanoregulation to guide the design of physical therapies[23,24] aiming to gain or preserve

bone mass[25-27], would reach very different conclusions if different theories of bone mechanoregulation are used. Therefore, understanding the mechanism of bone mechanoregulation in the physiological loading scenario is important.

The aim of the present study is to investigate the mechanism of bone mechanoregulation under the physiological loading, i.e., investigating the correlation between the rate of changes in bone densitometric parameters (quantified from *in vivo* μCT images) and the bone mechanical parameters (estimated from subject specific finite element models of mouse tibia) when the tibia is subjected to physiological loading.

2. Materials and Methods

2.1. *Quantification of the changes in densitometric parameters of mouse tibia*

The *in vivo* μCT image datasets collected from the NC3Rs project were used in this study to quantify the changes in densitometric parameters of mouse tibia. In summary, ten 13-week-old C57BL/6J female mice were purchased from Harlan Laboratories (Bicester, UK). They were housed in the University of Sheffield's Biological Services Unit with a twelve-hour light/dark cycle at 22°C and free access to food and water. At 18-week-old, some mice were given a daily intraperitoneal injection of PTH (hPTH 1-34, Bachem, Bubendorf, Switzerland) at 100ng/g/day 7 days a week. PTH was prepared in 1% acetic acid and 2% heat inactivated mouse serum in HBSS (Hank's Balanced Salt Solution, Gibco®). The treatment lasted until 22-week-old (the end of experiment). Based on the intervention, the mice were divided into wild type (WT, N = 5) and PTH treated (PTH, N = 5) groups. The entire right tibia of the mouse was scanned using an *in vivo* μCT imaging system (vivaCT 80, Scanco Medical, Bruettisellen, Switzerland) (**Figure 1**). A baseline scan was performed at week 14, and then follow-up weekly scans were performed starting from week 16 until week 22. The scanner was operated at 55 keV, 145 μA, 32 mm FOV, 1500/750 samples/projections, 200ms integration time and a nominal isotropic image voxel size of 10.4 μm. A third-order polynomial beam hardening correction algorithm, which was provided by the manufacturer and determined using the 1200 mg HA/cm^3 wedge phantom, was applied to all the scans. The image grayscale values were converted into HA-equivalent volumetric bone mineral density (BMD) values using the calibration law suggested by the manufacturer and based on weekly quality check performed using a five-rod densitometric calibration phantom. All the procedures were complied with the UK Animals (Scientific Procedures) Act 1986, reviewed and approved by the local Research Ethics Committee of the University of Sheffield (Sheffield, UK).

At the mouse age of 14 weeks, the axial growth of C57BL/6J mouse tibiae is small but still significant. Therefore, a partitioning protocol, where the regions of interest were scaled between time points, was developed by assuming an affine growth along the proximal–distal (longitudinal) axis of mouse tibia.[28] As a result, the volume in the same partition compartment for the same mouse would change between time points but would be maintained at the same anatomical location. The partitioning protocol has been well documented in a previous study.[28] In brief, for every mouse, the 3D image dataset obtained

from the first scan (week 14) was translated to align its longitudinal axis to the z-axis of the image system and then rigid registration was used to assure that all the images were placed in the same reference system (Amira 5.4.3, FEI Visualization Sciences Group, France). All follow-up μCT scans were then aligned to their corresponding first scans in a stepwise registration manner **(Figure 2a-c)**. For every scan, the tibial length (defined as the distance between the most proximal and distal bone voxels in the tibial longitudinal axis) was determined and then a region of 80% of tibia length was cropped out starting from the distal end of the proximal growth plate and was chosen as the volume of interest (VOI) **(Figure 2c)**. The fibula was removed from the tibial VOI. The VOI was then partitioned into 10 sections in the longitudinal direction with an equal length. The resulting sections were further divided into four angular compartments centred at the centre of mass of every cross-section, and oriented in the medial, lateral, anterior, and posterior directions **(Figure 2d)**.

Before calculating the densitometric parameters, the grayscale images were firstly smoothed using a Gaussian filter (convolution kernel [3 3 3], standard deviation = 0.65) in order to reduce the effect of image noise. The bone mineral density (BMD), obtained using the approach of phantom calibration, was summed up over every compartment in order to provide the Bone Mineral Content (BMC) values at every anatomical location, at every time point, and for every animal. The grayscale image datasets were binarised using a threshold value, which is 25.5% of the maximal grayscale value. [29] Then Bone Volume (BV) and Total Volume (TV) were calculated for every compartment. In every compartment, BMD was calculated by dividing BMC by TV and Tissue Mineral Density (TMD) was calculated by dividing BMC by BV. All calculations were performed using an in-house developed Matlab script (Matlab v2015a, the Mathworks, Inc. USA).

2.2. *Quantification of mechanical parameters of mouse tibia*

In order to explore the correlations between the rate of changes in bone densitometric parameters and the bone mechanical parameters in the spatiotemporal space, the average values of mechanical parameters in every anatomical compartment at every time point were determined for every mouse. Strain energy density (SED) and the 1st principal strain (ε_1) were selected as the mechanical stimuli in the present study, because SED is a resultant bone stimulus widely used in literature and highly correlated to the activities of bone adaptation, and ε_1 is a parameter associated with mode I (opening) bone fracture, which is the principal mode of bone fracture.

To compute SED and ε_1 under physiological loading condition, subject-specific finite element (FE) models of mouse tibia for every mouse at every time point were generated **(Figure 2f)**. In detail, the image datasets of tibial VOI were first smoothed with a Gaussian filter (sigma = 1.2, support = 2.0) and then binarised into bone and background using a fixed threshold, i.e., 25.5% of the maximal grayscale value,[29] corresponding to the valley region between the two peaks in the histograms. Then a connectivity filter was applied to remove the unconnected bone islands in the binary images. The resulting dataset was directly converted into a μFE Cartesian, 8-node hexahedral element mesh using a well-

established procedure.[30] The mechanical properties of the mineralised bone tissue were assumed to be homogenous, isotropic, and linear elastic, with an elastic modulus of 14.8 GPa, and a Poisson's ratio of 0.3.[31,32]

Physiological loading condition was defined in the FE models. In brief, the proximal end of the mouse tibia was fully constrained and the resultant forces generated at the distal end during normal locomotion were worked out using an inverse dynamics analysis [33], in process of which an instantaneous static equilibrium between the ground reaction force and the force of calf muscle was assumed. In the analysis, the horizontal component of the ground reaction force in the medial-lateral direction was neglected assuming the hind-limb motion was planar. The resultant axial and anterior-posterior forces applied on the distal end of mouse tibia were calibrated by matching the average strains (predicted from FE models of 12-week-old female mice) with those reported by De Souza *et al.* who experimentally measured the strains at the same sites during normal locomotion in a 12-week-old female mouse (**Figure 3**).[14] Because the mouse used in the FE modelling is different from that used in the experiment, five FE models of mouse tibia were created and the predicted strains averaged over all the FE models were compared with the experimental measurements reported by De Souza et al. On the other hand, because it is not clearly the direction of the strains measured from the strain gauges in the experiment, both the principal strains and the strain along the longitudinal direction of mouse tibia were obtained from the FE modelling and compared with experimental measurements. The resultant forces were calibrated until a match between the FE predicted strains and the experimental measurements was reached, which resulted in a force of 1.0 N along the tibial longitudinal axis and a force of 0.02 N along the tibial anterior-posterior axis for a mouse at a weight of 24.0 mg. The resultant forces, determined from the calibration process, were then scaled to the weight of every mouse and applied on the distal end of mouse tibia for every FE model at every time point. The FE models were solved using Ansys (Release 14.0.3, ANSYS, Inc.) on a workstation (Intel Xeon E-5-2670. 2.60 GHz, 256 GB RAM). The FE predicted values of elemental SED and the ε_1 at the centroid of every element were then averaged over every anatomical compartment. These values were used as the mechanical stimuli in the investigation of bone mechanoregulation mechanism in the following sections.

2.3. *Statistical analysis*

The data from the wild type (WT) and PTH-treated (PTH) mouse groups were analysed separately. The changes in BMC, BMD and TMD over time were assumed to depend on individual mouse (MouseID), the age of mouse (MouseAge), the spatial location (Compartment) and the mechanical stimulus (SED and/or ε_1). This assumption is based on two reasons: first, every mouse has a significantly different initial BMC value and different evolutions of BMC over time; second, there is still a non-negligible skeletal growth in C57BL/J6 female mouse at 14-week-old, and the magnitude of skeletal growth is different in different regions of mouse tibia (e.g., the growth near the growth plates is larger than

that in the midshaft), and thus the inclusion of Compartment as an independent variable in the model is necessary in order to capture the region-dependent skeletal growth.

The changes in the bone densitometric parameters (BDP) (BMC, BMD and TMD) between two consecutive time points t_i and t_{i+2}, were calculated using the following equation:

$$\Delta \mathrm{BDP}(t_i) = \frac{\mathrm{BDP}(t_{i+2}) - \mathrm{BDP}(t_i)}{t_{i+2} - t_i}. \quad (1)$$

where, ΔBDP(t_i) and ΔBDP(t_{i+2}) are the changes in bone densitometric parameters (BMC, BMD and TMD) at the time point t_i and t_{i+2}, respectively.

Based on preliminary results, a time-step of two weeks was adopted as the best compromise between smoothness of ΔBMC and temporal resolution. The analysis was limited to the interval from week 18 to week 22, in order to ensure that both intervention groups were equally sampled (because PTH data were available only from week 18). This resulted in 40 (compartment) × 5 (mouse) × 3 (time interval) = 600 data points for each group of mouse.

The correlation between the rate of changes in BMC, BMD, and TMD and the MouseID, MouseAge, Compartment, and mechanical stimulus (either SED or ε_1), was analysed using one-way factorial analysis ANOVA. Shapiro-Wilk normality test was used to check the normality of the residuals, and Bartlett test was used to check the homoscedasticity. Only the first-order effect was considered. Type III marginal Sum of Squares was used to calculate the probability, hereinafter simply referred as *p*. All the analyses were conducted using the free program R (https://www.r-project.org/). Probability of type I error was set to α = 99%, i.e., $p < 0.01$ was considered statistically significant.

3. Results

3.1. *Validation of the strains predicted by the FE tibial model*

The strain values, predicted by the FE models at the locations where strain gauges were attached, were found to be in a good agreement with the experimental measurements **(Figure 4)**. The strain values, measured by De Souza *et al*., were -300 με at the medial site and 200 με at the lateral site. With the boundary conditions calibrated, the FE models predicted an average normal strain of -278 ± 21 με at the medial site, and 193 ± 18 με at the lateral site; and an average 3rd principal strain of -292 ± 20 με at the medial site, and an average 1st principal strain of 208 ± 17 με at the lateral site.

3.2. *Correlations between mechanical stimuli and bone adaptation parameters*

Tibial length continuously increased from week 14 to 22, but the magnitudes of increase were small in both groups. Taking the values at week 14 as baseline, tibial length increased by 3.21 % and 4.23% at week 22 in the WT and PTH groups, respectively (**Figure 5**). The distribution of the 1st principal strain and the strain energy density over mouse tibia did not vary too much either across the groups or across the ages (**Figure 6**).

All probabilities analysed by the ANOVA models are reported in **Table 1**. The MouseID had a significant effect on the variabilitiy of ΔBMC, ΔBMD and ΔTMD in both groups ($p < 0.001$), which confirms that every mouse behaved differently, and justifies the need for subject-specific FE models to calculate the mechanical stimuli. The effect of MouseAge on these densitometric parameters was significant ($p < 0.001$) in all analyses except for the BMC in the PTH group. In both groups, the effect of Compartment was significant for BMC and BMD ($p < 0.001$), but not for TMD ($p > 0.01$).

In both groups, ε_1 had a minimal effect on the variability of ΔBMC ($p > 0.01$). SED had a significant effect on the variability of ΔBMC only in the WT group ($p < 0.01$), and not in the PTH group ($p > 0.01$). In both groups, SED had a significant effect on the variability of ΔBMD in both groups ($p < 0.01$). However, ε_1 had a significant effect on the variability of ΔBMD only in the PTH group ($p < 0.01$), and not in the WT group ($p > 0.01$). In both groups, neither SED nor ε_1 had a significant effect on the variability of ΔTMD ($p > 0.01$).

4. Discussion and Conclusion

In the present study, the correlations between the rate of changes in bone densitometric parameters and the bone mechanical parameters were investigated in mouse tibia (subjected to physiological loading condition) using the approach of *in vivo* μCT imaging and subject-specific finite element modelling.

In the present study, the variations in three densitometric parameters were investigated, i.e., BMC, BMC and TMD. It should be noted that ΔBMC represents the changes in bone mass caused by both bone modelling and remodelling; ΔBMD mostly represents the changes induced by bone adaptation at the porosity level and ΔTMD represents the changes induced by bone adaptation at the tissue mineralisation level. It is revealed in the present study that MouseID is significant in all ANOVA models, indicating the importance of subject-specific modelling. MouseAge is significant in most ANOVA models except for ΔBMC in the PTH group. The reason for this exception could be that PTH treatment boosts the increase in BMC[34] and the effect of treatment is so strong that it flattens the effect of time and age. The spatial compartment is significant in most ANOVA models except for ΔTMD in both WT and PTH groups, which indicates that tissue mineralisation (represented by TMD) changes over time (MouseAge) but not across the anatomical space (Compartment). The result that ΔTMD has no correlation with either SED or ε_1 implies that the rate of change in bone mineralisation could be primarily regulated by mouse age, and that the degree of bone mineralisation is not altered during bone adaptation. This result is in agreement with literature data [34, 35, 36].

Regarding the mechanical parameters, it is revealed in the present study that SED significantly contributes to the variability of ΔBMD in both WT and PTH groups. It has been found in the previous studies that the changes in BV/TV are significantly correlated with SED under para-physiological loading.[12] However, to the best of the authors' knowledge, the present study is the first to provide the evidence that the rate of changes in BMD is significantly correlated with SED under physiological loading. Considering the

average loads (and the associated strains) are fairly low (average strains around 600 με) under physiological loading, challenges to the idea of "Lazy Zone" are also raised, i.e., a range of SED values that do not elicit any mechano-adaptation response.[4] However, it should be noted that the observation in the present study is a limited phenomenon (i.e., for very small SED values) under the influence of many confounding factors, and thus the statistical significance that supports the conclusions is somehow modest.

The results on the 1st principal tensile strain (ε_1) are more complex to be interpreted. ε_1 was found to be significantly correlated with ΔBMD in the PTH group, but not in the WT group. There are two possible interpretations for this observation: the first one is that PTH stimulus amplifies the bone response in BMD to the mechanical stimulus, and thus pushes the mechanical indicators (SED and ε_1) to be significantly correlated with ΔBMD. In other words, the PTH stimulus acts as a confounding factor; the second possible explanation is that different mechanisms of bone mechanoregulation may coexist in reality, but predominately at different loading levels. In the WT group, the response to ε_1 is so small that it gets shadowed by the much stronger response of SED, whereas in the PTH group, the increased sensitivity of bone mechanoregulation makes both effects evident. It would be much more challenging to confirm such combined theory than the binary falsification of one versus the other, because of two main reasons: first, a modified longitudinal protocol needs to be developed to quantify not only the changes in BMC, but also the micro-cracks induced in the mineralised matrix and the number of Bone Remodelling Units activated at every time step. Both of these can be quantified only histologically, and thus some new methods that allow an indirect non-invasive estimation would be required. Second, para-physiological conditions need to be induced so that the repair-related and the non-repair-related bone remodelling events can be regulated somehow independently. This poses considerable challenges, and calls for future research.

It should be noted that in the present study, the homogeneous μFE models instead of heterogeneous models are used. There are two main reasons for this: first, the local value of bone mineral density in every voxel may be affected by image noise and it has been showed in a previous study that the BMC vales at the image voxel level (10.0 μm) are not reproducible, but have a good reproducibility over a larger bone volume of interest (much larger than the image voxel size); [28] second, one previous study showed that the tissue mineralization was stable in both WT and PTH groups across mouse tibia from week 14 to week 22[34] and thus homogeneous and heterogeneous μFE models could be equivalent in capturing the longitudinal changes in bone mechanical behaviour.

There are a couple of limitations related to the present study. First, there might be unknown effect of ionising irradiation (due to the *in vivo* μCT imaging) on the densitometric and mechanical properties of mouse tibia. However, considering the fact that all animals received the same amount of irradiation, even if there is a systemic effect of imaging irradiation, it can be assumed that the effect would be the same across the mice compared. Second, a homogeneous longitudinal growth of mouse tibia was assumed in the present study, while in reality the long bone grows in an anisotropic way that bone formation is progressed from the epiphyseal plate to the region of midshaft. However, the magnitude of increase in tibial length was small in both groups: taking the values at week 14 as reference, the maximal increases were 3.21% and 4.23% in the WT and PTH groups,

respectively. Therefore, the influence of assuming a homogeneous longitudinal growth of mouse tibia on the results, presented in the present study, is minimal.

In summary, it is revealed in the present study that under physiological loading condition, the correlations between the rate of changes in BMD and BMC and the mechanical parameters (SED and ε_1) are different in the WT and PTH groups, and ΔTMD has no significant correlation with either SED or ε_1 in both groups. This study is the first to explore the mechanism of bone mechanoregulation in the physiological loading scenario. However, the results are preliminary and more future investigations on this topic are needed to guide the design of physical therapies aimed to gain or preserve bone mass.

Acknowledgments

This work was funded by the National Natural Science Foundation of China (11702057, 11772086), the Chinese Fundamental Research Funds for the Central Universities (DUT15RC(3)130), the Open Fund from the State Key Laboratory of Structural Analysis for Industrial Equipment (GZ1611), Dalian University of Technology. Fruitful discussions with Prof. Marco Viceconti and Dr. Enrico Dall'Ara are also well acknowledged.

The raw data analysed and reported in this paper are obtained from the project funded by the UK National Centre for the Replacement, Refinement and Reduction of Animals in Research (NC3Rs), grant number: NC/K000780/1. The raw data are available in Open Access under CC-BY-NC license and can be retrieved with the following DOI: 10.15131/shef.data.3814701.

Conflict of Interest

The authors declare that they do not have any financial or personal relationships with other people or organisations that could have inappropriately influenced this study.

References

1. Frost HM, *The laws of bone structure*, Springfield, Thomas, 1964.
2. Cook SD, Skinner HB, Weinstein AM, Haddad RJ Jr, Stress distribution in the proximal femur after surface replacement: effects of prosthesis and surgical technique, *Biomater Med Devices Artif Organs* **10**(2):85-102, 1982.
3. Engh CA, Bobyn JD, Glassman AH, Porous-coated hip replacement. The factors governing bone ingrowth, stress shielding, and clinical results, *J Bone Joint Surg Br* **69**(1):45-55, 1987.
4. Huiskes R, Weinans H, Grootenboer HJ, Dalstra M, Fudala B, Slooff TJ, Adaptive bone-remodeling theory applied to prosthetic-design analysis, *J Biomech* **20**(11-12):1135-1150, 1987.
5. Carter, Mechanical loading histories and cortical bone remodelling, *Calcif Tissue Int* **36** S1:

S19-24, 1984.

6. Mullender MG, van der Meer DD, Huiskes R, Lips P, Osteocyte density changes in aging and osteoporosis, *Bone* **18**(2):109-113, 1996.
7. Burr DB, Forwood MR, Fyhrie DP, Martin RB, Schaffler MB, Turner CH, Bone microdamage and skeletal fragility in osteoporotic and stress fractures, *J Bone Miner Res* **12**(1):6-15, 1997.
8. Turner CH, Robling AG, Mechanisms by which exercise improves bone strength, *J Bone Miner Metab* **23**:16-22, 2005.
9. Schulte FA, Lambers FM, Kuhn G, Müller R, In vivo micro-computed tomography allows direct three-dimensional quantification of both bone formation and bone resorption parameters using time-lapsed imaging, *Bone* **48**(3):433-442, 2011.
10. Schulte FA, Zwahlen A, Lambers FM, Kuhn G, Ruffoni D, Betts D, Webster DJ, Mueller R, Strain-adaptive in silico modelling of bone adaptation – a computer simulation validated by in vivo micro-computed tomography data, *Bone* **52**:485-492, 2013.
11. Levchuk A, Zwahlen A, Weigt C, Lambers FM, Badilatti SD, Schulte FA, et al., Large scale simulation of trabecular bone adaptation to loading and treatment. *Clin Biomech* 29: 355-362, 2014.
12. Lambers FM, Kuhn G, Weigt C, Koch KM, Schulte FA, Müller R, Bone adaptation to cyclic loading in murine caudal vertebrae is maintained with age and directly correlated to the local micromechanical environment, *J Biomech* **48**(6):1179-1187, 2015.
13. Birkhold AI, Razi H, Weinkamer R, Duda GN, Checa S, Willie BM, Monitoring in vivo (re)modelling: a computational approach using 4D microCT data to quantify bone surface movements, *Bone* **75**:210-221, 2015.
14. De Souza RL, Matsuura M, Eckstein F, Rawlinson SC, Lanyon LE, Pitsillides AA, Non-invasive axial loading of mouse tibiae increases cortical bone formation and modifies trabecular organization: a new model to study cortical and cancellous compartments in a single loaded element, *Bone* **37**:810-818, 2005.
15. Willie BM, Birkhold AI, Razi H, Thiele T, Aido M, Kruck B, Schill A, Checa S, Main RP, Duda GN, Diminished response to in vivo mechanical loading in trabecular and not cortical bone in adulthood of female C57Bl/6 mice coincides with a reduction in deformation to load, *Bone* **55**(2):335-346, 2013.
16. Razi H, Birkhold AI, Weinkamer R, Duda GN, Willie BM, Checa S, Aging leads to a dysregulation in mechanically driven bone formation and resorption, *J Bone Miner Res* **30**(10):1864-1873, 2015.
17. Schulte FA, Ruffoni D, Lambers FM, Christen D, Webster DJ, Kuhn G, Müller R, Local mechanical stimuli regulate bone formation and resorption in mice at the tissue level, *PloS One* **8**(4):e62172, 2013.
18. Simske SJ, Guerra KM, Greenberg AR, Luttges MW, The physical and mechanical effects of

suspension-induced osteopenia on mouse long bones, *J Biomech* **25**(5):489-499, 1992.

19. Cowin SC, Hedgedus DH, Bone remodelling I: theory of adaptive elasticity, *J Elast* **6**:313-326, 1976.
20. Hedgedus DH, Cowin SC, Bone remodelling II: small strain adaptive elasticity, *J Elast* **6**:337-352, 1976.
21. Martin RB, Burr DB, A hypothetical mechanism for the stimulation of osteonal remodelling by fatigue damage, *J Biomech* **15(**3):137-139, 1982.
22. Prendergast PJ, Taylor D, Prediction of bone adaptation using damage accumulation, *J Biomech* **27**(8):1067-1076, 1994.
23. Dai R, Ma Y, Sheng Z, Jin Y, Zhang Y, Fang L, Fan H, Liao E, Effects of genistein on vertebral trabecular bone microstructure, bone mineral density, microcracks, osteocyte density, and bone strength in ovariectomized rats, *J Bone Miner Metab* **26**(4):342-349, 2008.
24. Lv J, Sun X, Ma J, Ma X, Xing G, Wang Y, Sun L, Wang J, Li F, Li Y, Involvement of periostin-sclerostin-Wnt/beta-catenin signalling pathway in the prevention of neurectomy-induced bone loss by naringin, *Biochem Biophys Res Commun* **468**(4):587-593,2015.
25. Cikrikcioglu MA, Sekin Y, Halac G, Kilic E, Kesgin S, Aydin S, Ozaras N, Akan O, Celik K,Hamdard J, Zorlu M, Karatoprak C, Cakirca M, Kiskac M, Reduced bone resorption and increased bone mineral density in women with restless legs syndrome, *Neurology* **86**(13):1235-1241, 2016.
26. Santos WR, Santos WR, Paes PP, Ferreira-Silva IA, Santos AP, Vercese N, Machado DR, de Paula FJ,Donadi EA, Navarro AM, Fernandes AP, Impact of strength training on bone mineral density in patients infected with HIV exhibiting lipodystrophy, *J Strength Cond Res* **29**(12):3466-3471, 2015.
27. Paliologo T, Shimano RC, Shimano AC, Macedo AP, Falcai MJ, Issa JP, Effects of swimming associated with risedronate in osteopenic bones: An experimental study with ovariectomised rats, *Micron* **78**:40-44, 2015.
28. Lu Y, Boudiffa M, Dall'Ara E, Bellantuono I, Viceconti M, Development of a protocol to quantify local bone adaptation over space and time: quantification of reproducibility, *J Biomech* **49**(10):2095-2099, 2016.
29. Klinck RJ, Campbell GM, Boyd SK, Radiation effects on bone architecture in mice and rats resulting from in vivo micro-computed tomography scanning, *Med Eng Phys* **30**(7):888-895, 2008.
30. Chen Y, Pani M, Taddei F, Mazzà C, Li X, Viceconti M. Large-scale finite element analysis of human cancellous bone tissue micro computer tomography data: a convergence study, *J Biomech Eng* **136**(10):101013, 2014.
31. Webster DJ, Morley PL, van Lenthe GH, Müller R, A novel in vivo mouse model for mechanically stimulated bone adaptation – a combined experimental and computational

validation study, *Comput Methods Biomech Biomed Engin* **11**(5):435-441, 2008.

32. Vickerton P, Jarvis JC, Gallagher JA, Akhtar R, Sutherland H, Jeffery N, Morphological and histological adaptation of mouse and bone to loading induced by repetitive activation of muscle, *Proc Biol Sci* **281**(1788):20140786, 2014.
33. Prasad J, Wiater BP, Nork SE, Bain SD, Gross TS, Characterizing gait induced normal strains in a murine tibia cortical bone defect model, *J Biomech* **43**(14):2765-2770, 2010.
34. Lu Y, Boudiffa M, Dall'Ara E, Liu Y, Bellantuono I, Viceconti M,, Longitudinal effects of Parathyroid Hormone treatment on morphological, densitometric and mechanical properties of mouse tibia, *J Mech Behav Biomed Mater*, 25(75)： 244-251, 2017.
35. Easley SK, Jekir MG, Burghardt AJ, Li M, Keavey TM. Contribution of the intra-specimen variations in tissue mineralization to PTH- and raloxifene-induced changes in stiffness of rat vertebrae. *Bone* 46: 1162-1169, 2010.
36. Campbell GM, Bernhardt R, Scharnweber D, Boyd SK. The bone architecture is enhanced with combined PTH and alendronate treatment compared to monotherapy while maintaining the state of surface mineralization in the OVX rat. *Bone* 49: 225-232, 2011.

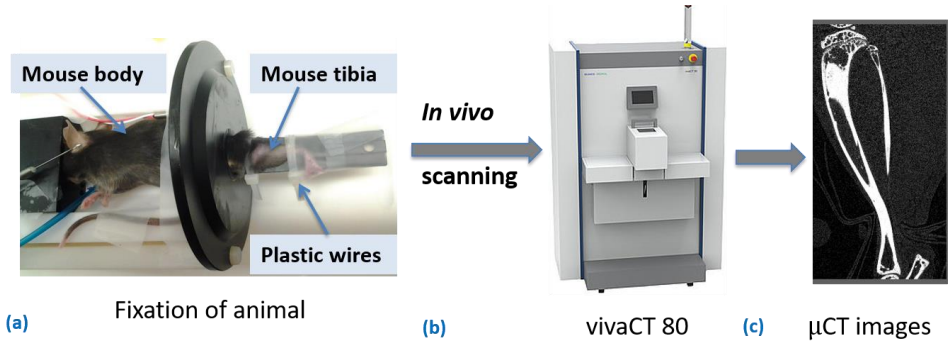

Fig. 1. Workflow for obtaining the µCT images of mouse tibia. The mouse was anesthetized and the tibia was fixed (a). The entire tibia was scanned using the system of vivaCT 80 (b). The µCT images at the resolution of 10.0 µm were obtained.

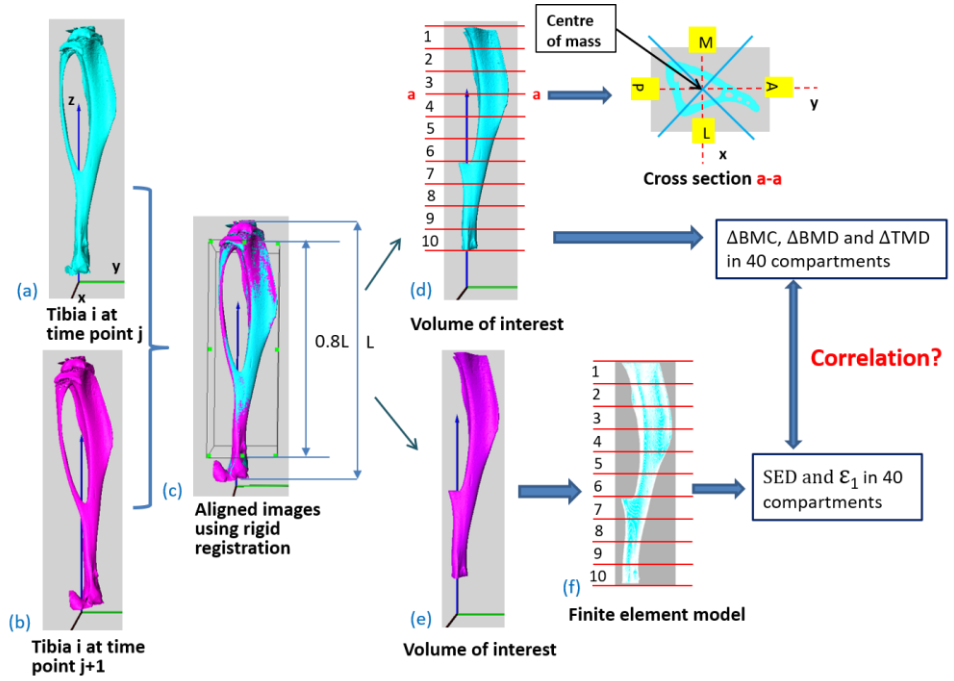

Fig. 2. Workflow for investigating the correlations between the rate of changes in densitometric parameters and the mechanical parameters of mouse tibia. The tibiae were processed and partitioned into 40 compartments (a - d). First, they were rigidly registered using a stepwise manner (a, b and c). A region of 80% of the entire tibia was selected as the volume of interest (VOI) and partitioned into 40 compartments (d). Finite element (FE) models were generated from tibial VOIs and the results were partitioned into 40 compartments accordingly (f). Then, the correlation between the the rate of changes in tibial densitometric parameters and its mechanical parameters were investigated in the spatiotemporal space. (In the figure, A, M, P and L represents Anterior, Medial, Posterior and Lateral, respectively)

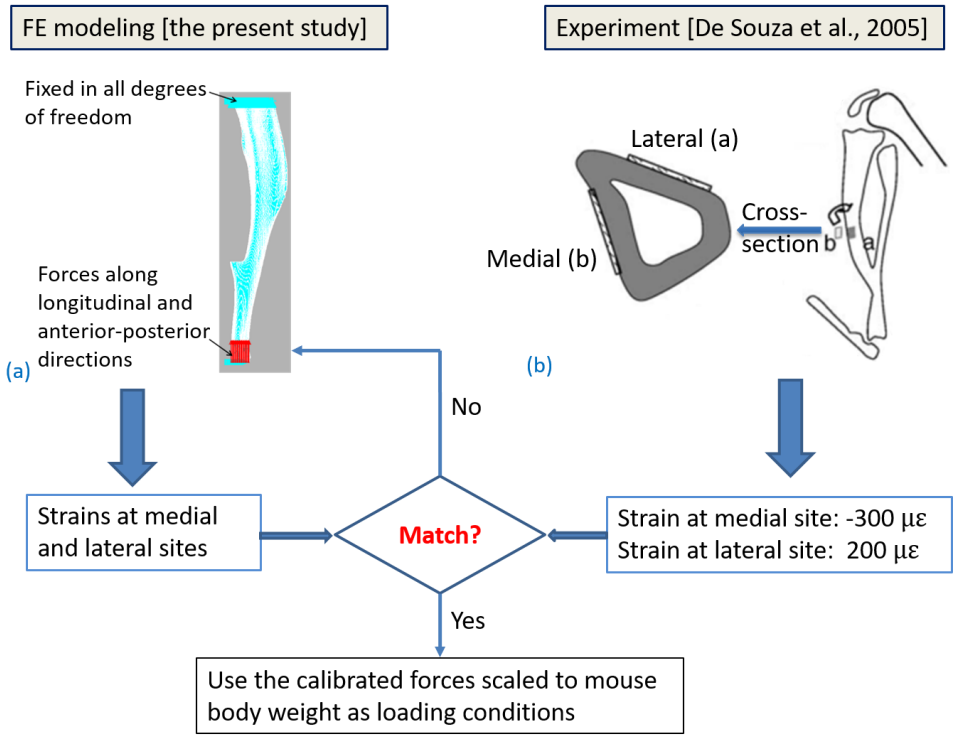

Fig. 3. Workflow for the determination of physiological loading condition defined in the finite element (FE) model of mouse tibia. FE model of mouse tibia was created (a) and the strains at the locations where strain gauges were attached during experiment were extracted. The strain values predicted by the FE model were compared with the corresponding experimental values (b) recorded during normal locomotion. The forces defined in the FE model were calibrated until the values between the FE prediction and the experimental measurement were close to each other.

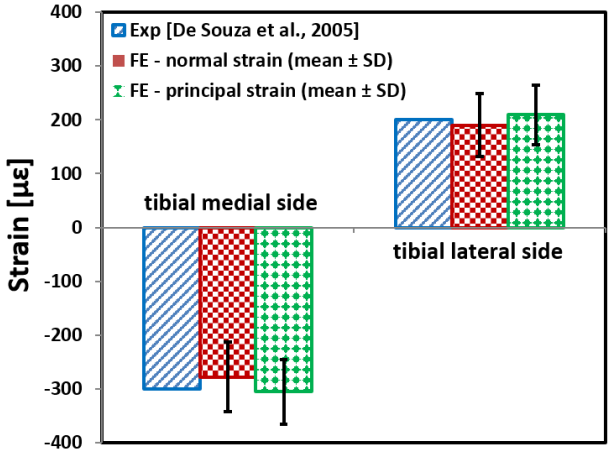

Fig. 4. Comparisons of the *in vivo* experimental data with the strains predicted by the finite element (FE) models of mouse tibia. The data of FE simulations are presented as the mean ± one standard deviation.

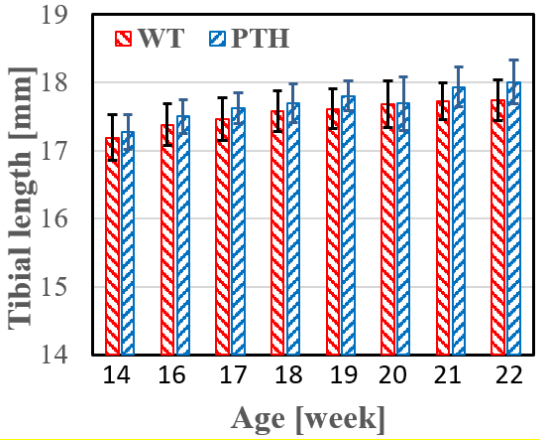

Fig. 5. The longitudinal changes of tibial length in the WT and PTH groups. Data are presented as the mean ± one standard deviation of tibial length in the WT and PTH groups.

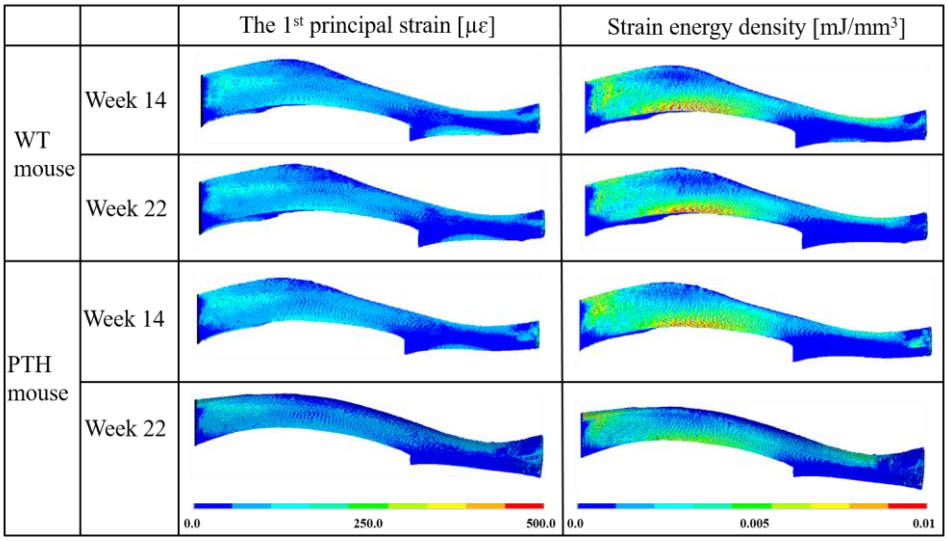

Fig.6. Distribution of the 1st principal strain and the strain energy density over mouse tibiae. All the images of mouse tibiae were plotted with the same view angle. The images of week 14 and 22 came from the same mouse in the WT and PTH groups, respectively.

Table 1. Probability values (*p*-values) for all the ANOVA models (significant values are highlighted in bold)

Groups	Dependent Variable	MouseID	MouseAge	Compartment	SED	ε_1
WT	ΔBMC	**7.37e-08**	**4.03e-15**	**< 2.2e-16**	**0.0061**	
WT	ΔBMC	**2.60e-08**	**8.17e-16**	**< 2.2e-16**		0.1087
WT	ΔBMD	**6.11e-16**	**< 2.2e-16**	**< 2.2e-16**	**0.0021**	
WT	ΔBMD	**3.05e-16**	**< 2.2e-16**	**< 2.2e-16**		0.1014
WT	ΔTMD	**1.61e-03**	**2.42e-03**	0.2007	0.8734	
WT	ΔTMD	**1.57e-03**	**1.94e-03**	0.1824		0.8285
PTH	ΔBMC	**< 2.2e-16**	0.7610	**2.55e-14**	0.2417	
PTH	ΔBMC	**< 2.2e-16**	0.9380	**6.75e-14**		0.9445
PTH	ΔBMD	**4.70e-14**	**< 2.2e-16**	**6.96e-14**	**3.16e-05**	
PTH	ΔBMD	**< 2.2e-16**	**< 2.2e-16**	**< 2.2e-16**		**4.07e-08**
PTH	ΔTMD	**3.68e-08**	**1.26e-15**	0.0112	0.0122	
PTH	ΔTMD	**1.03e-07**	**8.51e-15**	0.1080		0.0826